MRes – The Science and Engineering of Materials

Deformation of inclusions in rail steel due to rolling contact

Alison Chard

[redacted]

January 2011

Abstract

Rolling contact fatigue (RCF) is a significant problem in the rail industry as it causes rapid and difficult to detect cracks. Inclusions present in the material can have an adverse effect on the RCF life of rails.
This study aims to discover the impact of the loading of rail steel in service on the inclusions present within the material. The work pays particular attention to the elongation and flattening of MnS inclusions and their contribution toward rail failure using a combination of micro-hardness measurements, inclusion analysis and focused ion beam analysis.
The results indicate that the inclusions present in the material are considerably elongated by the loading of the rail in service and this may contribute to spontaneous cracking or assist in crack propagation.

Table of Contents

1. Introduction.....4

2. Literature review.....5

2.1. Rail-wheel interaction and contact stresses.....5

2.2. Rail Steels.....8

2.2.1. Pearlitic rail steel.....8

2.3. Work Hardening of pearlitic rails.....13

2.4. Inclusions in rail.....15

2.5. Rail Fatigue.....17

2.5.1. Rolling Contact Fatigue (RCF).....17

2.5.2. Head Checks.....18

2.5.3. Squats.....19

2.5.4. Crack Initiation.....19

2.5.5. Crack Propagation.....20

2.6. Literature Review Conclusion.....22

3. Aims and Objectives.....24

4. Experimental Method.....25

5. Results.....27

6.1. Hardness..... 27

6.2. Inclusion Measurements..... 29

6.3. Shear Angles.....31

6.4. Inclusion Composition.....32

6.5. Focused Ion Beam.....33

6. Conclusions.....36

7. Acknowledgements.....38

8. References.....38

1. Introduction

The trains that use the UK's rail network are getting heavier and they're running more often. This combination of heavier axle loads and more frequent loading on the rail tracks has lead to higher demands on the rail steel that makes up the UK's extensive rail network. As a result the rails experience plastic deformation in the contact zone, where the wheel exerts most force on the rail, which results in wear and rolling contact fatigue crack initiation.

Figure 1 shows the number of defective and broken rails removed from service since 1965.

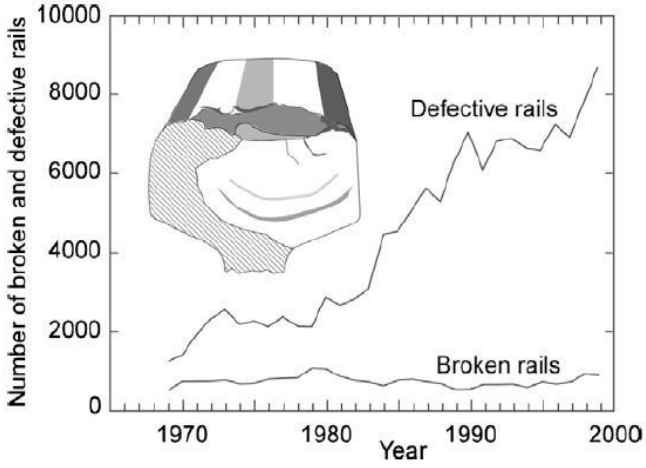

Figure 1: Long term trend of broken and defective rails removed in Railtrack railroad Network (Zerbst, 2009).

2. Literature review

2.1. Rail-wheel interaction and contact stresses

The life of a rail in service depends on the abrasive wear it experiences and the fatigue damage it suffers (Hans Muster, 1996). Harder rails experience less abrasive wear but can fail due to rolling contact fatigue (RCF). This is because the surface layers of the rails are not removed by wear processes allowing cracks to propagate.

As a railway vehicle wheel passes over the rail the rail steel is exposed to high stresses, which typically reach 1500 MPa for a 25 tonne load (Zerbst, 2009) causing deformation and work hardening. The load of the passing trains on the steel exceeds the yield stress of the rail steel which is typically around 410 MPa (Zerbst, 2009), resulting in plastic deformation. In more detail this involves the differences in yield strength between the ferrite and cementite that make up the rail's pearlitic structure; this will be discussed later. The cementite is a much harder phase than the ferritic phase in the pearlite. This means that deformation of the structure does not happen uniformly and when exposed to stresses above those of the yield strength of the pearlite cracks can initiate between the ferrite and the cementite due to their mechanical differences. This is an important point to consider as it means cracks can initiate and grow from points in the bulk of the material out towards the surface (Wetscher, 2007). This difference in mechanical properties of the constituent phases of the pearlite resulting in internal cracking of the pearlite is the exhaustion of ductility. Each train passing over the rail will plastically deform the rail track. As a number of subsequent trains pass over the same piece of rail track progressive deformation will occur resulting in the exhaustion of ductility exhaustion of ductility and therefore initiation of rolling contact fatigue cracks discussed above. As a maintenance procedure the rails are ground down to maintain a good head profile. This also removes the surface cracks associated with RCF however with each grinding material is removed from the head of the rail. This results in a reduction in the bending fatigue strength of the rail which continues to

reduce with increasing grinding maintenance operations.

As the wheel moves along the rail there will be rolling contact and partial slip rolling which occur due to frictional effects between the wheel and rail. Once the friction is overcome sliding contact becomes more significant. These three factors are responsible for the deformation and work hardening of the rail as well as wear (Telliskivi, 2001). As the contact patch and associated stresses are so important in determining the wear and deformation of the rail there have been many models developed with the purpose of gaining a greater understanding of rail- wheel interaction (Telliskivi, 2001). Using modelling it has been found that the contact stresses when the wheel is in contact with the rail are higher than the ultimate tensile stress of the rail steel itself (Telliskivi, 2001). Although this is determined from models it still shows that when the rail is under loading from the wheel it is experiencing severe conditions.

The area over which the rail and wheel make contact is known as the contact patch, contact stresses arising in this contact patch locally affect both rail and wheel. The rail and wheel profile along with the type of train all affect the size and shape of the contact patch (Vasić, 2011). The size of the contact patch can be calculated from the normal force, the material properties, wheel geometry and the rail (Iwnicki, 2003). Although the contact patch varies the ellipse has been reported to have a diameter of 6-8 mm both in length and width, around the size of a 10p piece (Garnham, 2008). The Hertzian contact model is used to describe forces generated in the contact patch on a straight length of track. The Herzian theory is only valid for elastic contacts however it has been found to describe the local forces generated in the contact patch well despite the plastic nature of the contact between rail and wheel. The model is believed to apply so well as initially the plastic deformation of the contact patch will be small and with the passing of more trains the rail will quickly work harden to the extent that further plastic deformation of the contact zone will be prevented, this is known as shakedown (Zerbst, 2009). As the contact patch can no longer deform it can essentially be described as Herzian so the Herzian model

applies. On a curved piece of track, however, Herzian theory does not apply as for straight pieces of track. This is because the contact patch on a straight piece of track is located at the top, centre point of the rail head. It is known as non-conformal contact, this term is used to describe contact between two convex surfaces in this instance the curved wheel and the rounded rail head. On a curved piece of track the contact is known as conformal. In this instance contact is made closer to the edge of the rail head so that the surfaces of the rail head and the wheel have a more similar radius. Conformal contact results in much higher stresses so the plastification of the contact patch cannot be negated as it was in the case of non-conformal contact. The geometry of the contact patch is also different in conformal contact from the ellipse -shaped contact patch used in Hertzian calculations on straight rail (Zerbst, 2009). Within the contact patch longitudinal and transverse creepages occur, which will again be dependent on the wheel profile and rail section such as a corner or straight section (Garnham, 2008). RCF life is generally reduced by an increase in transverse creep due to curving forces and therefore with corner rail sections (Garnham, 2008). Figure 2 shows the differences in contact stresses depending on the position of the wheel on the rail.

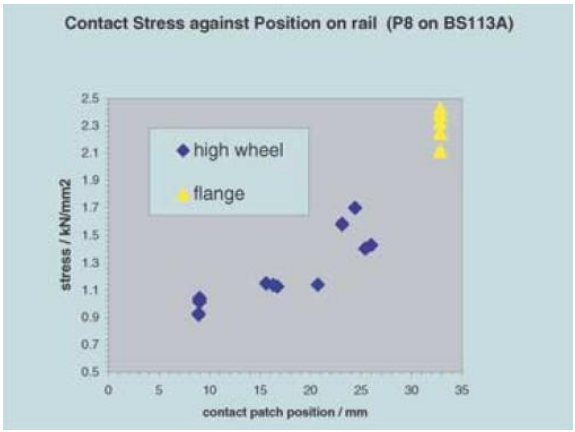

Figure 2: Predicted contact stress against position on the rail head for the Class 43 locomotive in 700m to 1800m radius curves (From Iwnicki, 2003).

2.2. Rail Steels

2.2.1. Pearlitic Rail Steel

The UK's extensive railway network requires a large amount of track to be installed and maintained and therefore the cost of the material is significant. Rail steels should be tough, hard and strong because wear and fatigue control the life of rails in service. Pearlitic steels are most commonly used in the UK rail network. Pearlite has the capacity to work harden significantly so it can become very high strength in service. The work hardening of rail steel will be discussed in more detail later in this section. Other steel phases could be used however they lack the variety of properties that pearlite has, for example martensite is initially a harder material than pearlite however the high strength, high carbon martensites are too brittle so do not meet the toughness requirements, low carbon martensitic steels meet the toughness requirements of the pearlitic rail steels however they cannot work harden in service as much as pearlitic steels so lack the required in service strength. Highly alloyed martensitic steels can combat this problem but would be too expensive. The rail material must be as resistant to cracking as possible whilst meeting the other requirements, ferrite is more resistant to cracking than pearlite however it has poor wear characteristics. It can be seen that the choice of material for the rails is a compromise of properties. A harder material or a tougher material could be used but other properties would be too seriously compromised to make that material choice feasible. Pearlite has a good spread of properties meeting aof the material requirements of the rail however there is always the search for better materials which has lead to the use of bainitic rail steels in some areas of the world (Jin, 1997).

Bainitic materials are considered more suitable for heavy-duty rails and as such have successfully been used in railway crossings (Shariff, 2011). Bainitic steels are made up of plates or laths of ferrite containing elongated Fe_3C particles. Upper bainite is formed at higher temperatures than lower bainite and contains carbides outside of the ferrite laths. Lower bainite contains smaller carbides ouside of the ferrite laths but cabides are present inside the laths. Bainitic steels derive their strength from a high density of

dislocations i.e a greater number of smaller precipitates gives a stronger steel whereas pearlitic steels gain their strength depending on grain size and interlamellae spacing (Aglan, 2006). Bainitic steels are initially harder than pearlite which it was thought would improve the rail's wear characteristics. In practice however some investigations find that due to the poor work hardening ability of bainite this is not the case (Chang, 2005), see Figure 3 showing bainite wears to a much greater degree than fully pearlitic rails (Hernandez, 2007. Shariff, 2011). Other studies however have found that bainitic steels may actually wear as well as normal pearlitic rail steels as well as being more ductile and having a better toughness (Chang, 2005). It is thought that studies showing the poor wear resistance of bainite can be put down to other phases being present in the material resulting in a mixed microstructure.

Lower bainite or a mixture of upper and lower bainite (Shariff, 2011) is thought to be more suitable than upper bainite for rails. Upper bainite generally contains coarse carbide precipitates resulting in poor ductility and a tendency to crack. Carbides are also present in lower bainite and it is important to remove them with the addition of silicon. The resulting carbide-free steel contains bainitic ferrite, retained austenite and maybe also some martensite depending on the process (Chang, 2005). The carbide-free lower bainite steels had better tensile strength, impact resistance and wear resistance than bainite containing carbide precipitates (Chang, 2005). The retained austenite is present in much higher volumes than in lower carbon steels, around 17% and in low carbon steels around 6% (Chang, 2005) however due to wear most of this is converted to martensite. This resulted in a transformational hardening of the bainitic steel. This transformational hardening has been recognised as an effective way to improve the wear resistance of bainite (Chang, 2005).

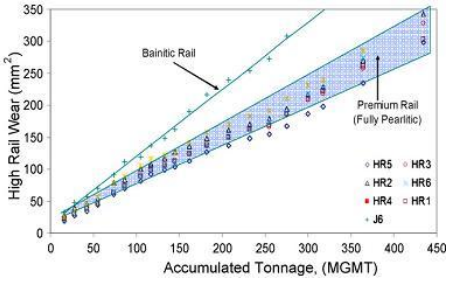

Figure 3: Showing the difference in wear rates for pearlitic and bainitic rail steel (From Hernandez, 2007).

Other comparisons between pearlitic and bainitic rails have found that the bainitic steels exhibited 'superior flaking resistance, good wear resistance and excellent weldability' (Aglan, 2006). Bainitic steels have a higher fracture toughness than pearlitic steels, 50-60 MPa $m^{1/2}$ against 30-35 MPa $m^{1/2}$. This higher fracture toughness means that bainitic steels can withstand larger crack lengths so would need less maintenance (Aglan, 2006)

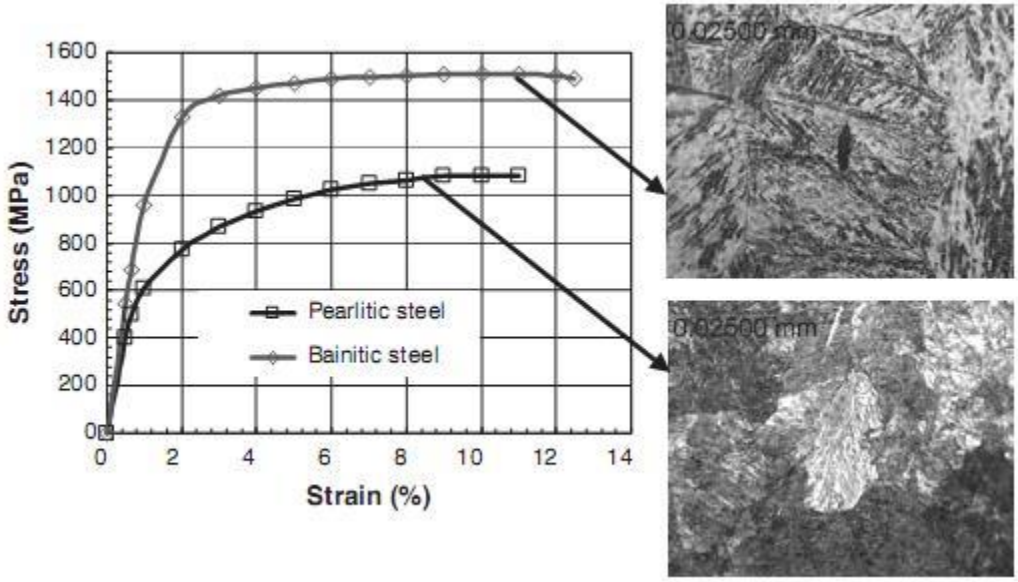

Figure 4: Stress - strain curve for pearlitic and bainitic steel along with their microstructures (Aglan, 2006).

Figure 4 shows the different microstructure and it can be seen that the bainite is made up of particles of cementite in a ferrite matrix. By decreasing the bainite transformation temperature the number of cementite particles can be increased whilst the average size of the particles will be reduced. This results in a stronger material than the pearlite. Figure 5 shows that the higher fracture toughness associated with the bainitic rail steel results in a much slower crack growth.

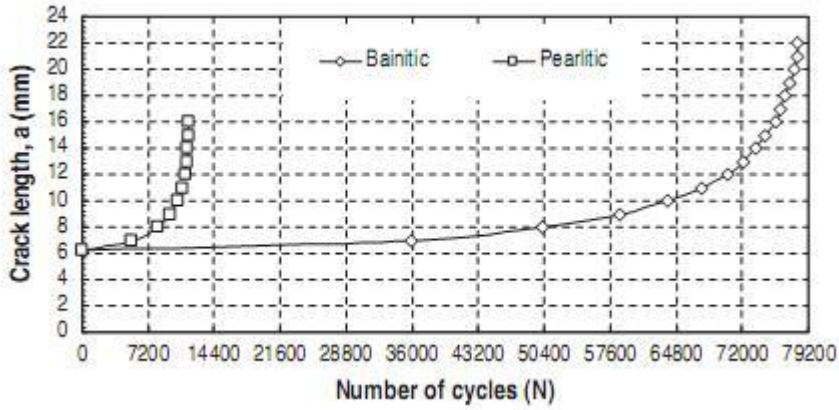

Figure 5: A graph showing crack length depending on number of cycles for bainitic and pearlitic steels based on the averages from 3 macroscopically identical specimins (Aglan, 2006).

Pearlitic rail steel typically contains 0.5-1wt% carbon and is made up of alternating layers of soft ferrite and hard cementite (Fe_3C). It can be seen in the phase diagram in Figure 6 that the pearlite is formed from the cooling of the austenitic phase and depending on the amount of carbon in the pearlitic steel there may be pro-eutectoid ferrite or pro-eutectoid cementite formed. The presence of these phases will impact negatively upon the overall properties.

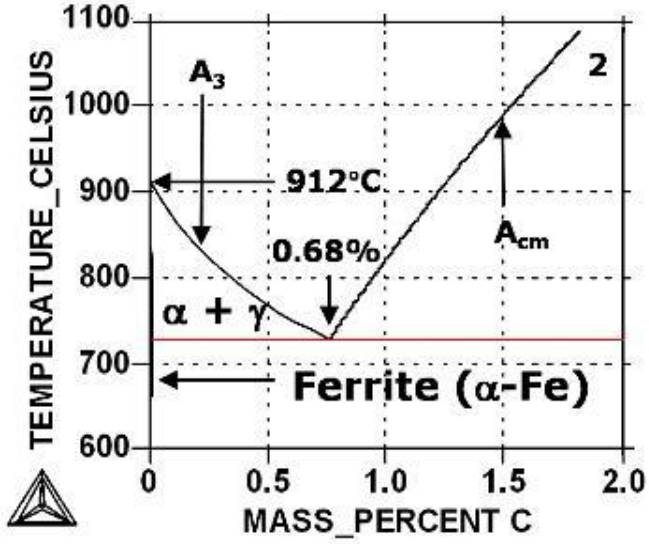

Figure 6: The Iron-Carbon phase diagram. From http://www.calphad.com/graphs/Metastable%20Fe-C%20Phase%20Diagram.gif

As the pearlite is formed of layers of cementite and ferrite there can be variation in how thick the layers are and this is known as the interlamellar spacing. The smaller the interlamellar spacing the harder the material will be. The steel grades most commonly used in the UK are 220 which has now been superseded by 260 grade, compositions given in Table 1 below. Both 220 and 260 grade rails are predominantly pearlite however pro-eutectoid ferrite forms along grain boundaries in the 220 grade. This pro-eutectoid ferrite is not present in such large amounts in 260 grade steel as the higher carbon and manganese content promote a fully pearlitic structure. The microstructure also contains inclusions such as MnS, SiO_2 and Al_2O_3.

Table 1: The composition (wt%) of 220 and 260 steel grade rail steels, From the Institute of Rail Welding

Steel	C	Si	Mn	S	P	Cr	Mo	Ni	Cu	Al	N	O	V	Ti
UK 220	0.50 0.60	0.20 0.60	1.00 1.25	0.008 0.025	MAX 0.025	MAX 0.15	MAX O.02	MAX 0.10	MAX 0.15	MAX 0.004	MAX 0.008	MAX 20ppm	MAX 0.03	MAX 0.025
UK 260	0.60 0.82	0.15 0.58	0.65 1.25	0.008 0.025	MAX 0.025	MAX 0.15	MAX O.02	MAX 0.10	MAX 0.15	MAX 0.004	MAX 0.01	MAX 20ppm	MAX 0.03	MAX 0.025

Grade	0.2% Proof Stress (MPa)	UTS (MPa)	Elongation (%)	Hv
UK 220				220-260
UK 260	502	954	12	260-300

2.3. Work hardening of pearlitic rails

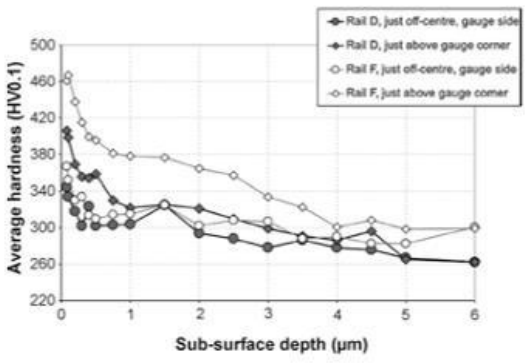

Figure 7: Near surface strained region of micro hardness curves for SUROS tests to run to RCF failure at 150 MPa contact stress and -1% creepage (from Garnham, 2008)

Work hardening is a cold deformation process that happens to the surface of rails through rail-wheel contact (Wetscher, 2007). The deformation and resulting work hardening change the mechanical properties of the steel. The fact that pearlitic steels have the capacity to work harden and therefore increase significantly in hardness at the surface is a major advantage of using pearlitic steels for rails. The undeformed structure of pearlite consists of alternating lamallae of ferrite and cementite. The finer the lamallae of ferrite and pearlite the harder the steel. The pearlite structure is randomly orientated in the undeformed rail. When pearlite is subjected to loading it deforms and work hardens. This hardening is a result of the unaligned pearlite becoming aligned in the direction of the loading i.e. parallel to the rail surface (Wetscher, 2007).

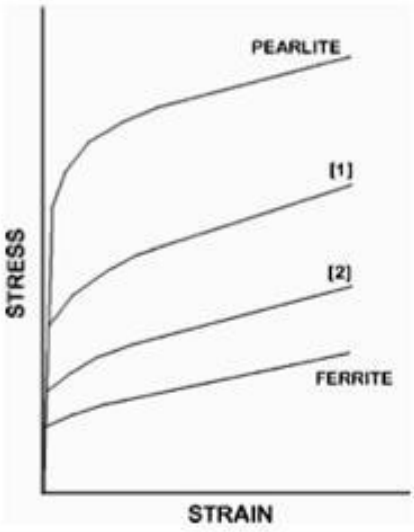

Figure 8: Schematic stress-strain curve for 100% ferrite, 100% pearlite, (1) highly constrained, thin pre-eutectoid ferrite zone in a ferrite-pearlite matrix and (2) lightly constrained, thich pro-eutectoid ferrite zone in a ferrite-pearlite matrix (from Garnham, 2008).

The compressive loading the pearlite undergoes varies with distance from the surface. The surface of the rail will be more heavily loaded. This gives rise to a hardness profile where hardness of the rail changes with depth, which is shown in Figure 7 for rails removed from service.

The surface of the rail becomes more severely deformed throughout its lifetime (F. Wetscher, 2007). The material is deformed incrementally with each passing train and it eventually reaches its ductility limit.

and begins to crack (Franklin, 2008). Cracks have been found to initiate in the pro-eutectoid ferrite. The preferential straining of pro-eutectoid ferrite, as the softer phase, compared to the pearlite results in cracking which decreases the fatigue life of the rail (Garnham, 2008). The difference in strain between PE ferrite and pearlite can be seen in Figure 8 which shows the stress strain curve for 100% pearlite and 100% ferrite. The difference between the yield points can be clearly seen.

As the volume fraction of PE ferrite is reduced and the steel becomes fully pearlitic, the PE ferrite can no longer play a part in crack initiation. This is the reason for the move to 260 steels in place of 220 steels. Inclusions in the steel such as MnS can then become significant crack initiators (Dhua, 2000).

2.4. Inclusions in rail

Large brittle inclusions, such as those containing Ca, Al, Si and O can initiate critical cracks below the surface of the rail head (Garnham, 2010). Brittle inclusions cause fatigue cracking in two ways; they can directly nucleate cracks as they do not deform in line with the surrounding matrix material and by causing micro-cracks at the interface between the inclusion and the matrix (Dhua, 2000). During service these cracks can propagate and result in failure. As such the rail industry have worked to reduce the size and number density of these inclusions. As the problems associated with brittle inclusions are reduced attention has been turned to soft ductile inclusions, in particular MnS.

There are a number of inclusions present in the rail steels of the compositions in Table 1. The most common of which are MnS, Al_2O_3 and SiO_2. The inclusions present in the steel on solidification are initially spherical and varying in diameter.

A study (Liu, 1993) found, when looking at four different pearlitic rail steels after deformation, that Al-containing inclusions remained small and circular whereas MnS inclusions became elongated. Other inclusions were also found in the deformed steel such as Al_2O_3 stringers and hard angular SiO_2. Those inclusions containing alumina and silica are possibly more likely to initiate cracks as the inclusions themselves are brittle so under loading they can shear in a brittle manner. As this is known, during the manufacture of rail steel care is taken to avoid the formation of these inclusions. The study (Liu, 1993) concluded that those steels with high sulphur contents contained higher number densities of MnS inclusions.

The 260 grade steels, composition given in Table 1, tend to have fewer but larger inclusions than the 220 grade rail steels and these inclusions are orientated in the longitudinal direction (Ory, 2008). The steel is then rolled to give that rail profile, which elongates the inclusions in the rolling direction, so the inclusions go from spherical to oval/ cigar shape (Garnham, 2008). In general it is found that most inclusions in rail steel are longitudinally orientated and differ in size. The rails are then put into service. In service the surface of

the rail deforms most and so do the inclusions. The inclusions do not deform in a uniform way, the longitudinal loads exceed the transverse loads which results in the formation of a flattened, pancake inclusion close to the surface which can become crack initiation sites (Garnham, 2008). This large inclusion deformation is most associated with MnS inclusions as they are highly ductile when compared to SiO_2 and Al_2O_3. Further work (Liu, 1993 and Keissling, 1978) using micro-hardness testing to measure the MnS inclusions found that MnS inclusions in a pearlite matrix had a micro-hardness of 175 kg/mm^2. In contrast the pearlitic steel matrix was found to have a micro-hardness of 322 kg/mm^2 (for a 20g applied load). Pure MnS was found to have a micro-hardness of 170 kg/mm^2 showing the validity of the micro-hardness tests (Keissling, 1978).

The values above are taken from pure MnS however depending on the sulphur content of the steel and the steel making process other elements may well be present in the MnS inclusion changing the way the inclusion behaves (Garnham 2010). These inclusions can be made up of a ductile MnS part alongside a brittle inclusion e.g. alumina- silicate or the inclusion can be a ductile MnS inclusion surrounded by a brittle phase or a brittle phase surrounded by ductile MnS (Garnham, 2010).

From this section it can be seen that the MnS inclusions present in rail steel deform more than the surrounding matrix when under an applied load causing the inclusions to flatten and elongate.

2.5. Rail Fatigue

Damage to the rail as a result of wear processes can easily be seen meaning it is a safe form of rail damage. Rail fatigue on the other hand is much more problematic as it difficult to see and if left unmonitored can result in rail failure (Garnham, 2007).

Fatigue cracks can initiate at the head, web or foot of the rail but this work will focus on those at the rail head. Over time the fatigue cracks can grow and cause the rail to fail. There are a number of common crack types which will be discussed in this section.

2.5.1. Rolling Contact Fatigue (RCF)

Rolling contact fatigue (RCF) damage is caused by the action of the wheel rolling over the rail. RCF damage can lead to rail replacement or total failure and its effects can be reduced by reducing the stresses on the rail, rail grinding, using cleaner steels and regular inspection (Beynon, 1996).
There are a large variety of vehicle types, axle loads, vehicle speeds and contact geometries; this makes an absolute understanding of RCF difficult. When pro-eutectoid ferrite is present the RCF resistance is found to be decreased (Franklin, 2008) i.e. fully pearlitic steels have a higher RCF resistance. It was found (Garnham, 2007) that RCF crack initiation and propagation in steels containing both the pro-eutectoid ferrite and pearlite phases was accelerated due to strain partitioning between the phases with the pearlite phase gaining a greater degree of hardening and the pro-eutectoid ferrite phase reaching the exhaustion of its ductility. Cracks have been found to initiate between the two phases. These RCF cracks can then propagate rapidly in the highly strained region between the pro-eutectoid ferrite and work hardened pearlite.

2.5.2. Head checks

Head checks usually occur at the gauge corner as a series of surface cracks typically spaced 0.5-10 mm apart (Zerbst, 2009). These cracks are a problem precisely because they occur as a series. One crack at or approaching critical length is surrounded by other cracks growing in a pre-damaged section of steel. Several cracks at critical length can cause total failure of the rail. This is what is thought to have caused the Hatfield disaster in 2000 (Zerbst, 2009). Head checks are formed because the wheel causes gross plastic deformation as it passes over the track (Zerbst, 2009).The material between the cracks that make up the head check can spall away but as the cracks grow they can travel in a transverse direction to cause failure of the rail. Figure 9 below shows head checks.

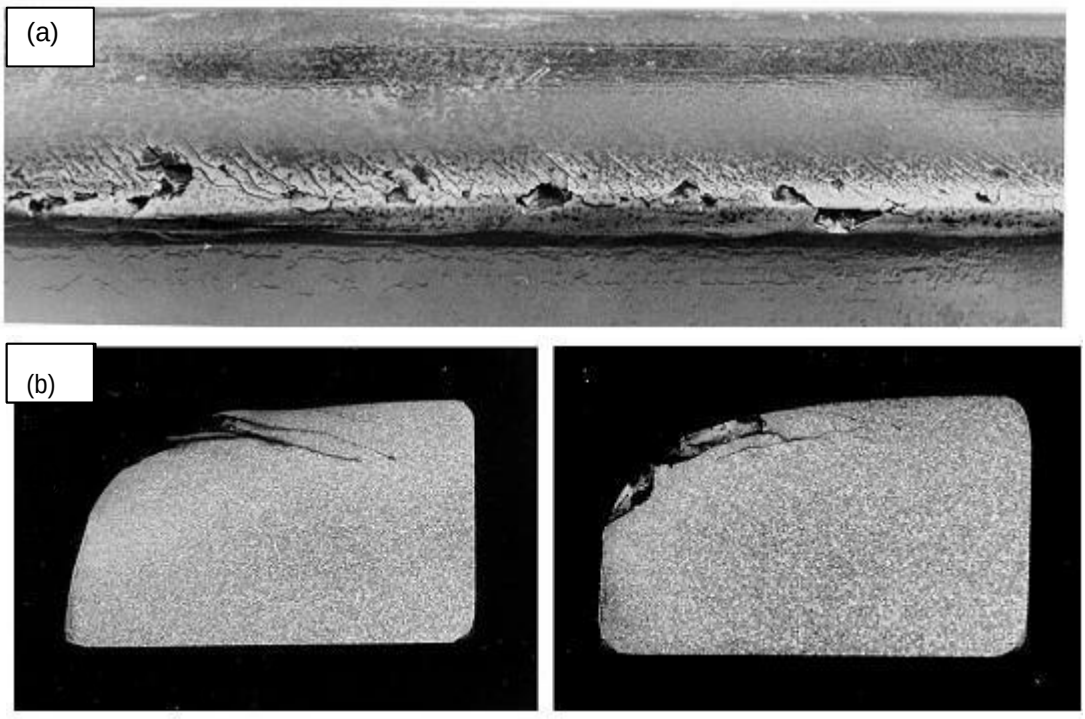

Figure 9: (a) spalling originating at head checks and (b) early propagation of a head check at a transverse section. From Zerbst, 2009

2.5.3. Squats

Squats occur at the running surface in isolation unlike head checks, squats are however also caused by gross plastic deformation (Zerbst, 2009). Squats initially grow at an angle to the running surface as shown in Figure 10 before turning to the transverse direction.

Figure 10: Early propagation of a squat in a longitudinal section. From Zerbst, 2009

2.5.4. Crack initiation

Rail wear is a much more predictable process than crack initiation by RCF, which can be rapid and the resulting cracks difficult to detect. The cracks are nucleated by cycling large plastic strains at the surface of the rail head due to the load from the train acting in the contact patch on the rail; this process is known as ratchetting (Zerbst, 2009). This crack initiation begins in the microstructure of the steel and is therefore affected by grain boundaries, precipitates and inclusions. The plastic deformation from the passing trains gives rise to dislocations within the grains of the surface rail steel. This plastic deformation is then continued as more trains pass over the rails and this causes slip bands to form. These slip bands are surrounded by material that is less deformed. The further deformation of the slip bands results in the formation of a crack (Zerbst, 2009). Any imperfections in the materials such as the inclusions commonly found in UK rail steels can act as stress concentrators and therefore aid or be responsible for the nucleation of cracks although to what extent inclusions are detrimental to fatigue crack initiation is not known. Despite this it has been found that cracks most commonly occur at the surface of the rail in the very highly strained, and therefore very thin, ferrite bands which can act as ‘planes of weakness’ (Garnham, 2008). Cracks

can also initiate along the highly strain flattened MnS inclusions (Franklin, 2008 & Ghorem, 1982. It is thought that there are three ways that inclusions can act as crack initiators; Firstly they could cause micro-crack initiation at localised deformation bands ahead of inclusions or secondly they could cause interfacial debonding due to high stress concentrations in the middle of elongated inclusions or thirdly brittle inclusions which break to act as cracks (Liu, 1993).

2.5.5. Crack propagation

After the crack has initiated and grown to a certain depth, which is dependent on the material type and applied load, the crack moved into the propagation stage. In this stage the rate at which the crack is growing accelerates (Zerbst, 2009). At this time the fatigue cracks still propagate due to contact stresses as well as bending and stresses induced by the load of the passing trains (Zerbst, 2009). These stresses are shown in Figure 11. The bending stresses shown in Figure 11 have both a vertical and lateral component and it is the vertical component of the bending stress that contribute most to the fatigue crack growth (Zerbst, 2009). It can also be seen in Figure 11 that there is a shear stress component which mainly causes crack growth where it gives rise to mixed loading conditions i.e. Mode II mechanism (Zerbst, 2009). The crack propagates in a mixture of mode I (opening) and mode II (sliding) mechanisms.

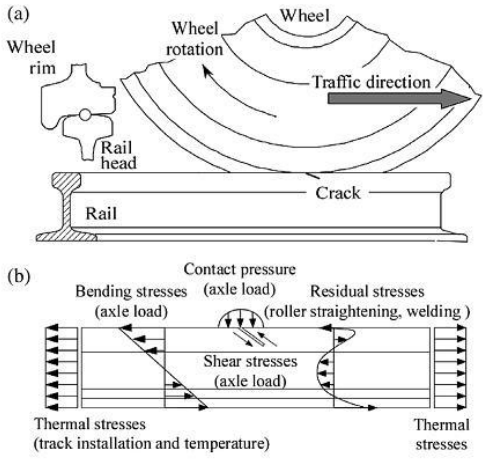

Figure 11: (a) A wheel rolling on a rail and (b) Contact stresses and longitudinal stress components. From Zerbst, 2009)

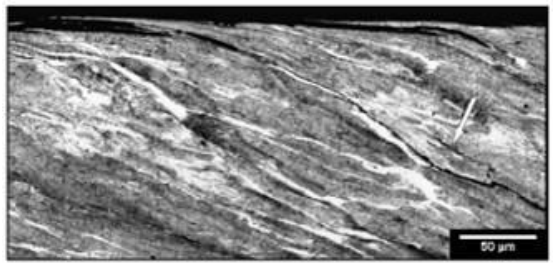

Figure 12: Optical micrograph shows crack initiation at the rail surface and propagation along the border of strained pro-eutectoid ferrite grain boundaries. The arrow shows branching to flattened MnS inclusions (Franklin, 2008).

As the crack grows larger still the crack tip moves away from the high stress areas and so the crack growth is not as driven by the rail- wheel contact stresses. At this point liquids, such as water or lubrication affect the growth direction and move the crack growth mechanism from Mode I &II to Modes II & III. This is because the liquids lubricate the crack surface which reduces friction. This shift to Mode II and III crack growth also corresponds to a branching of the crack. Figure 12 shows this crack propagation.

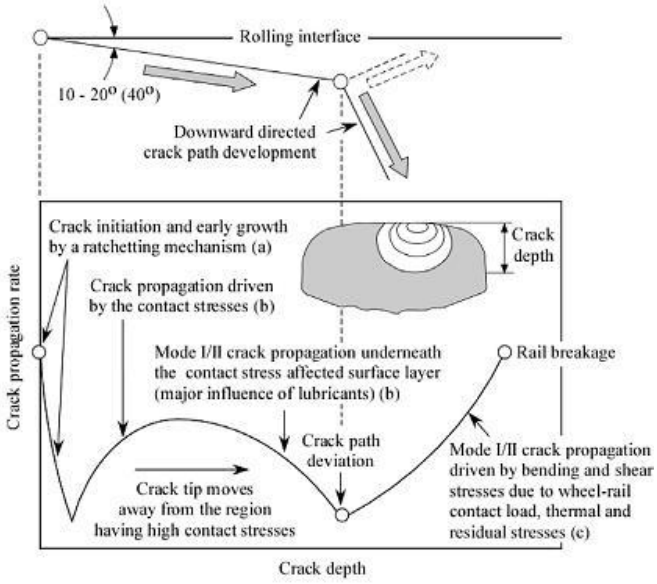

Figure 13: Propagation stages of a squat-like fatigue crack. From Zerbst, 2009.

It has previously been found that cracks smaller than 50um in length tended to follow strained pro-eutectoid boundaries in 220 grade rail steel. This was not found the be the case once the cracks had become larger (Garnham, 2008). Cracks generally propagate in the direction of the strain field however cracks can follow the ferrite grain boundaries (Franklin, 2008), as shown in Figure 13.

Figure 13 also shows that MnS inclusions present in the steel are routes for crack propagation as well as pearlite grain boundaries and strain field

direction. With fully pearlitic steels the MnS inclusions have been found to play a more important role in crack initiation and propagation (Franklin, 2008) because preferential pro-eutectoid ferrite straining is not a factor.

Following crack branching the crack grows at an angle to the surface of the rail (between 60-80 degrees) and now grows under Mode I loading conditions more than at the other propagation stages although Modes II and III do have an effect (Zerbst, 2009). Eventually the crack grows causing failure of the rail.

2.6. Literature Review Conclusion

From studying the literature available on rail steels, inclusions and rolling contact fatigue it can be seen that due to greater pressures on rail networks there is a great need to better understand the effects of inclusions and RCF on rails. Pearlitic steels are a good choice for rails as they have a good combination of properties and the ability to work harden. As the alternating layers of ferrite and cementite which make up pearlite are strained by passing trains the layers become thinner and it is this that results in work hardening. Bainitic steels are also used in certain applications although there are doubts about the wear resistance of the material as it does not work harden. As rail material is plastically deformed by successive trains exhaustion of ductility can result in the more ductile phase (ferrite). Cracks can initiate in the regions between ferrite and cementite due to differences in yield strengths between the materials. On curved pieces of rail the contact stresses in the contact patch are much higher than for a straight piece of track resulting in a higher likelihood of cracks forming in gauge corners.

Pearlitic steels contain inclusions and it is well known that inclusions are detrimental to the rail. The brittle inclusions present in steel have been reduced in number density and size as a result however ductile inclusions, primarily MnS are still present in high number densities. MnS inclusions can become crack initiators as they deform in a non-uniform manner to produce long thin inclusions.

RCF cracks are difficult to detect and monitor as they can often form spontaneously and grow beneath the surface of the rail. Inclusions present in the steel can act as or aid crack initiators and as the crack propagates through the rail due to the contact stresses induced by passing trains the MnS inclusions can act as crack propagation routes. Pro-eutectoid ferrite also acts in this way however it is not present in fully-eutectic rail steels which are now commonly in use.

3. Aim

3.1. This project aims to quantify the deformation of inclusions in the contact zone in rail removed from service with a view to understanding how near surface inclusion deformation affects crack initiation in rail steel.

4. Objectives

- Measure the vertical hardness profile of the rail to measure the depth of rail deformation.
- Measure the composition of the inclusions using EDX.
- Quantify the amount inclusions deform depending on depth using optical microscopy.
- Measure the nano-hardness difference between inclusions and the matrix to determine the inclusion deformation behaviour
- Measure the angle of shear associated with deformation of the microstructure due to rolling contact
- Determine the 3-D nature of deformed inclusions near surface using focused ion beam (FIB) measurements.

5. Experimental Method

A number of experiments have been carried out to further understand the rail microstructure, properties and deformation. The samples and techniques used will be discussed here.

The samples used were taken from a rail known as Rail E which was removed from service. The rail is a 260 grade steel whose composition is given in Table 1. This rail is likely to be a corner section of rail.

Hardness measurements were made using both transverse and longitudinal samples taken from Rail E. The samples were polished to 1μm finish. Micro-hardness indents were made, using a 200 g load, at 0.25 mm intervals vertically to a depth of 10 cm and repeated at 5 mm intervals horizontally across the transverse sample. Figure 14 shows a map of the indent locations.

The inclusions in the rail were characterised using optical microscopy. Using the results gained from the hardness measurements discussed above the inclusions from row D and H were characterised. Rows D and H were selected as areas of most and average wear respectively. The inclusions along the vertical indents at rows D and H, both transverse and longitudinal, were characterised by their Feret max, Feret min, Feret ratio and equivalent circle diameter using the KS400 software along with a Leica optical microscope.

The shear angles of the rail were investigated to further understand the rail deformation. Shear angles were measured by taking micrographs of the transverse samples for both row D and H using an optical microscope. The shear angles were then calculated taking the surface of the sample as 0 degrees.

Inclusion composition was measured using samples polished to a 1μm finish. The samples were viewed in a Jeol 6060 SEM and the composition was measured using EDX.

Focused Ion Beam (FIB) was used to measure inclusion profile through the steel. A highly deformed section was required so the measurements were performed on a section of longitudinal row H close to the surface. The sample was polished to a 1μm finish.

Nano hardness indents were attempted on a longitudinal sample at row H polished to a 1μm finish, however it was not possible to gain any viable results

6. Results and discussion

6.1. Hardness

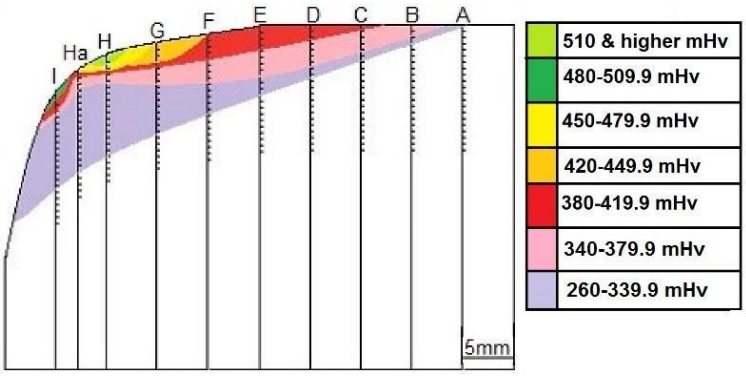

Figure 14: Hardness map for 260 grade transverse rail section

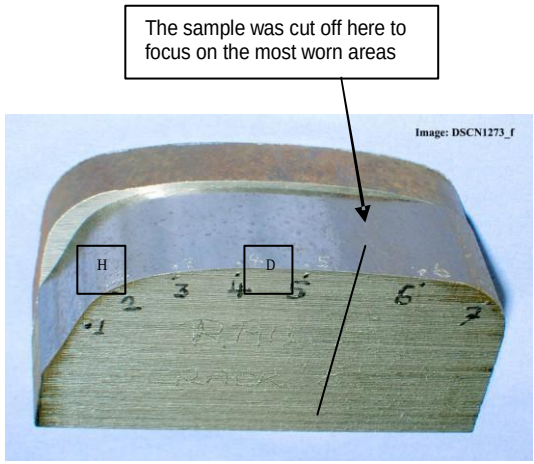

Figure 15: Shows the original rail profile against the worn profile of the rail from service (From J.E Garnham)

Micro-hardness testing was used to measure the work hardening of the rail. From these results the map shown in Figure 14 was created. The map clearly shows the variation in hardness values across the rail head. The surface of the rail head is harder than the bulk of the rail which means the loading done by the passing trains while the rail was in service has resulted in surface hardening.

This increase in hardness at the surface is not uniform. The greatest hardness increase can be seen at points H, Ha and I, this can be explained by the rail coming from a corner piece of track so loading, and therefore work hardening, would have been greatest at the gauge corner. Figure 15 also shows the wear at the gauge corner is greatest as most material has been worn away. The hardness at point A (furthest from the gauge corner) is lowest further supporting the variable contact experienced by the rail. The work hardening of the rail extends down to ~3 mm below the surface at the most greatly loaded point.

The highest hardness value was obtained at point H at the surface at 571.4 mHv and at point I 489.2 mHv again at the surface. When compared to the bulk material which was below 320 mHv this is a great increase of hardness due to work hardening. The variation in surface work hardening is also great. The surface point at A was 320 mHv so equal to the bulk which was not work

hardened. It is likely some of the work hardened surface material at point A has been worn away by work processes from passing trains however at all other points besides A there is some degree of work hardening which the passing trains do not wear away.
The colour on the hardness map stops when all values were in the purple range of 260-349 mHv.

Other research (Garnham, 2008) showed that rails work harden to depths of up to 6 mm which is greater than shown in the hardness map in Figure 14. This difference may be due to a difference in loading on the sections of rail tested.

6.2. Inclusion measurements

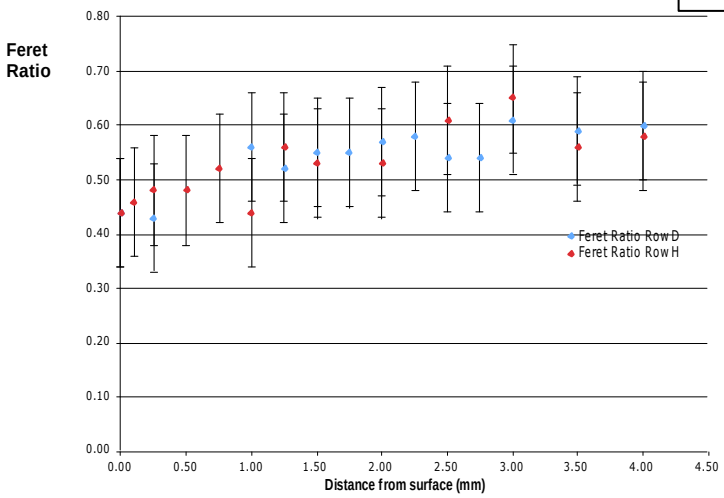

Figure 16: A graph of transverse inclusion Feret ratio with distance from surface for a 260 grade rail steel.

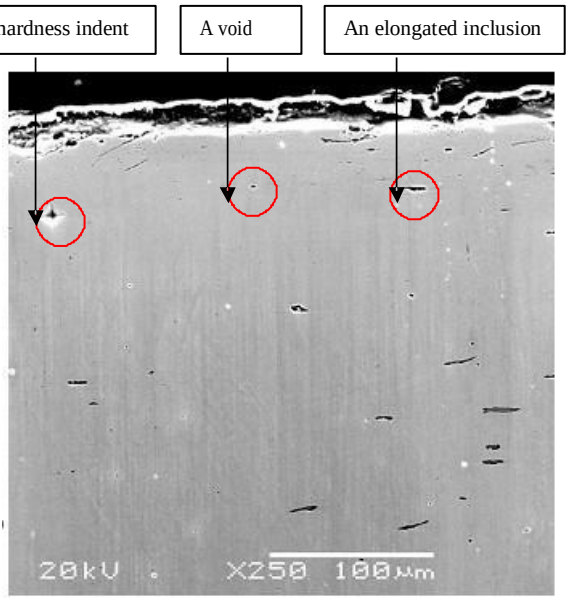

Figure 17: SEM micrograph of longitudinal section of 260 grade rail steel at row H. The inclusions are elongated parallel to the rolling direction

Two rows on Rail E were chosen for greater analysis based on the micro hardness results. Row H was chosen as the most severely deformed point and row D was chosen as it exhibits some work hardening but it is not severe.

Some small spherical pores can be seen in Figure 17. EDX was used to confirm they were not inclusions or a void left by an inclusion as there was no chemical difference between these pores and the matrix therefore they are a polishing effect. As they are not present in the bulk, only at the surface, any point with a Feret ratio of greater than 0.7 has been removed to prevent them affecting the data.

Figure 16 shows the variation in inclusion Feret ratio with distance from the surface. Feret ratio is a measure of the longest part of the inclusion over the widest part of the inclusion. The general trend of the graph is an increasing Feret ratio with an increasing distance from the surface. This means the inclusions are becoming more spherical away from the surface therefore the inclusions tend to be more elongated closer to the surface than in the bulk of

the rail. Row D inclusions are also less elongated than the inclusions in Row H. This is due to the increased loading of the material at Row H compared to Row D.

From the surface of the rail to 0.7 mm there is a large increase in Feret ratio showing that the inclusions at the very surface of the material are very heavily deformed compared to the inclusions further from the surface. The Feret ratio for the transverse samples levels out at a depth of around 3 mm which shows the loading of the trains is deforming the inclusions to a depth of 2-3.5 mm. This can be compared to the 3 mm work hardening depth from micro hardness measurements showing depth of work hardening and depth of inclusion deformation are linked. The deformation of the rail due to loading is both work hardening the steel and deforming the inclusions it contains to a similar depth.

The inclusion deformation in the longitudinal direction as shown in Figure 17 is striking when compared with the high Feret ratios seen in Figure 16. The very elongated inclusions are generally only seen in the longitudinal direction as inclusions are elongated in the direction of train travel. Table 2 below gives average values for inclusions in Rail E in both longitudinal and transverse orientations.

Table 2: Average size (Feret max) and Feret ratio of all inclusions taken from 4 random micrographs within the work hardened zone of Rail E.

Rail orientation	Feret max	Feret Ratio
Transverse	5.9 µm	0.54
Longitudinal	18.3 µm	0.29

6.3. Shear angles

6.3.1. Transverse

Table 3: Shear angle values with depth for transverse sections of 260 grade rail steel

	Transverse section	
Distance from surface (mm)	Shear angle Row D	Shear angle Row H
0.00	0	0
0.05	8	2
0.10	10	5
0.15	26	7
0.2	23	8
0.23	25	8
0.25	27	12
0.27	30	16
0.3	28	-
0.35	27	-
0.40	24	-
0.42	26	-
0.45	26	-

The surface of the rail is taken as 0 degrees. The angle of shear, shown in Table 3, increases with distance from the surface.

This shows the pearlite is becoming aligned parallel to the direction of rolling/ passing trains closer to the surface. The grains of pearlite are being compressed and forced in to one orientation from the loading action of trains. This would explain the severe work hardening seen at the surface of the rail as the cementite and ferrite layers are being rolled out and therefore compressed. This would reduce the interlamellar spacing resulting in work hardening.

Again rows D and H were analysed. Below 0.3mm for row H and 0.45 mm for row D it is very difficult to measure the shear angle because it is not as certain where the shear angle is no longer affected by loading. Due to this it is also difficult to compare the shear angle results to the hardness and inclusion results however it can be seen that shear angle is definitely affected to a depth of 0.3mm which correlates to the dramatic increase in Feret ratio for inclusions seen between 0mm and 0.25mm showing the most deformed inclusions are seen in the most deformed microstructure. This link between deformed pearlite close to the surface of the rail and very deformed inclusions close to the surface shows the inclusions are being deformed along with the microstructure and that in pearlite deformation of inclusions can be linked to work hardening.

6.4. Inclusion composition

Table 3: The composition of different points in a 260 grade rail steel measured using EDX

Inclusion type	Al	Si	S	Mn	Fe	No of points measured
Matrix	0.1	0.4	0.5	2.4	96.8	8
Void	0.1	0.4	3.9	10.6	85.0	9
Inclusion	0.1	0.1	31.5	56.1	12.3	2
Inc/Void 0	1	0.4	14.4	25.4	59.8	5

Table 3 shows that where analysis is done at the centre of an inclusion, labelled 'inclusion' on the table, the levels of both Mn and S are considerably higher than in the matrix. This shows the inclusions are mainly MnS although a more comprehensive EDX study would be needed to confirm.

The voids measured also contain levels of Mn and S which are above those seen in the matrix, this suggests the some of the voids once contained MnS, and these inclusions have become dislodged from the matrix. The inclusions labelled 'inc/void' are measure at the interface between an inclusion and the matrix, as would be expected the levels of Mn and S are halfway between those for the matrix and an inclusion.

6.5. Focused Ion Beam (FIB)

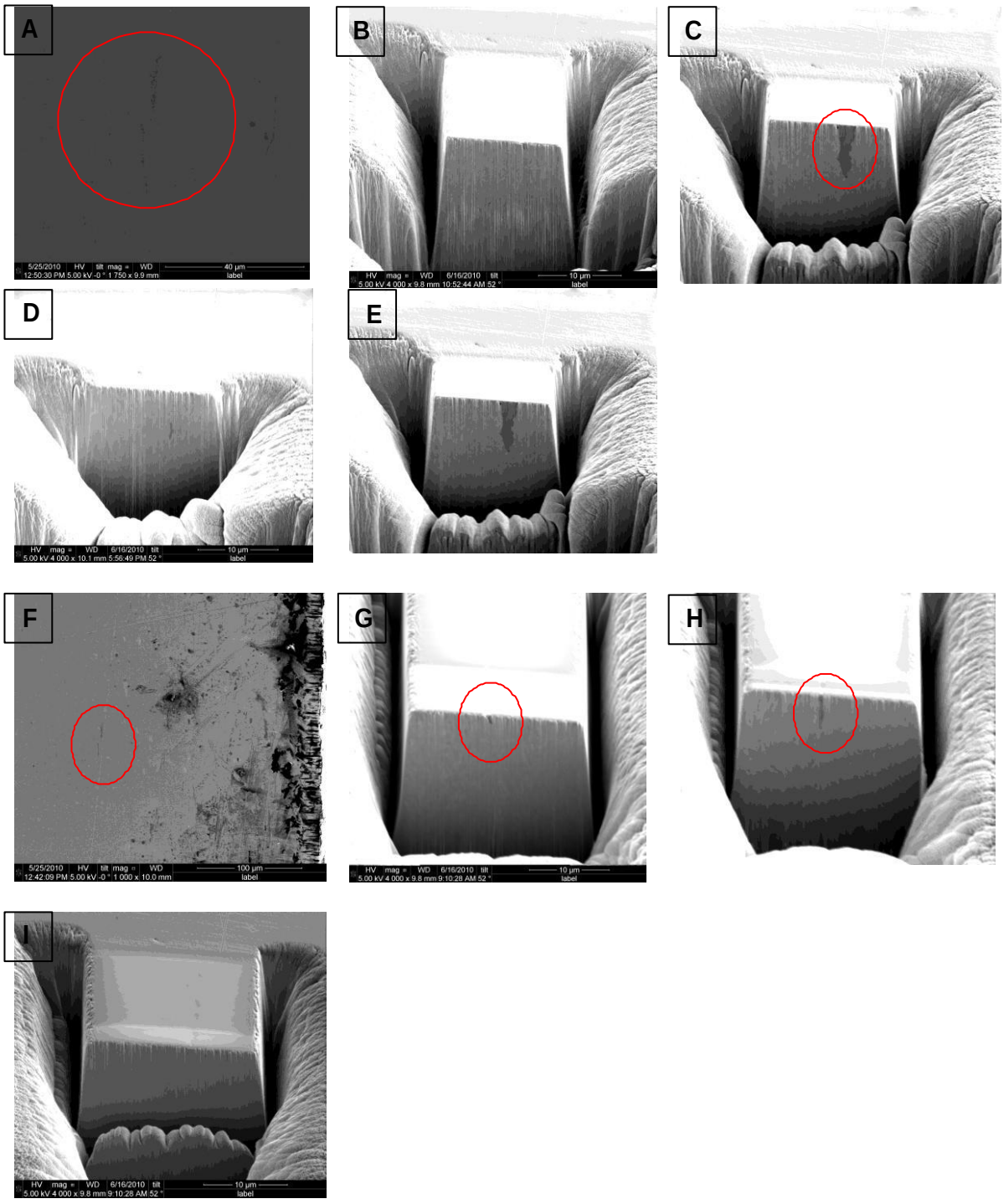

Figure 18: FIB Analysis of two inclusions. Images A-E show inclusion 1. A is the view of the inclusion at the surface, B is the starting point of FIB, C is the inclusion at its largest point, D is the final slice of the inclusion and E shows a viod at the edge of the inclusion. Images F-I show inclusion 2. F is the view of the inclusion at the surface, G is the first slice through the inclusion, H is the inclusion at its largest point and I is the final slice through the sample.

FIB analysis of three separate inclusions was made to determine the 3D nature of the inclusions. FIB was used to cut small slices through the inclusions to see if the inclusions deformed in a uniform manner through the material.

The micro hardness results showed the first 0.5 mm of the material was the most significantly work hardened when compared with material which was not work hardened 3 mm below the surface. As the inclusions chosen were small and none of them penetrated more than 5um into the material the micro hardness data showed they were all safely within the severely work hardened zone. The deformation looked for is from the difference in transverse and longitudinal loading.

FIB also has the advantage of showing voids around the MnS inclusion as shown in Figure 18. These voids show where the MnS and the metal surrounding it are coming apart and a crack will form. In general these voids are seen on the steep edged of the flattened inclusion so cracks are forming due to longitudinal stresses. No cracks can be seen, only the voids so it is not possible to say solely based on the FIB results in which direction these cracks would travel.

The FIB images showed that the MnS inclusion does not deform uniformly through the material. The slices show a constantly changing cross section of inclusion as shown in Figure 19.

Figure 19 shows an inclusion with an F max of 6.4 µm and an Feret ratio of 0.35 which is consistent with inclusions seen on 2D micrographs. The voids seen in the FIB images are also present in the 2D micrographs as can be seen in Figure 17. Figure 17 also shows the non-uniformity of the inclusions in the steel however it is much clearer on the 3-D images in Figure 19. The inclusions shown in Figures 18 and 19 also show the inclusions elongated normal to the rolling direction which relates to the shear angle data in Table 3 showing the rail deforming with the direction of train travel.

Figure 19: Successive FIB slices through rail steel showing the variation in inclusion deformation.

7. Conclusions

Rail E was taken from service and an initially comparing the sample to an new rail it could be seen that the rail was worn (Figure 15). Further investigation through micro hardness testing showed that the rail was work hardened to a depth of around 3 mm and that the rail was significantly work hardened at the gauge corner. This is because the rail was a corner piece of track. The rail was not uniformly work hardened along the surface showing where the surface had been more loaded. From this it can be concluded that the rail is significantly and non-uniformly work hardened due to the loading of trains in service.

Following micro hardness testing analysis was made at points D and H of the rail and it was found that inclusions near to the surface of the material were much more elongated than those found in the bulk of the material. This shows that as the rail deforms and the pearlite layers are compressed the MnS is also deformed. MnS is more ductile and has a lower hardness value than the surrounding pearlite matrix so significantly deformed in the matrix.

Analysis of shear angles showed that the pearlite is aligning with the direction of travel near to the surface and this means that the inclusions too are moving to that orientation. The inclusion composition was shown to be MnS with the use of EDX analysis.

FIB showed that the inclusions were not deforming in a uniform manner under in service conditions and small voids were seen to form which could suggest crack formation.

Overall measurements on rail E taken from service have shown that the inclusions present in this 260 grade steel are generally MnS and are highly elongated at the surface compared to those in the bulk. The inclusions are more elongated in the longitudinal direction than the transverse direction due to the higher stresses in the longitudinal direction during loading. The

loading of the rail results in work hardening whose effects extend further into the material than microstructural changes, measured by shear angle.

The experimental results coupled with the literature review in this work show that MnS inclusions are signifialnly affected by the loading and subsequent deformation of rails. The inclusions become highly elongated and highly deformed MnS inclusions have been shown in other work to be a significant factor in crack initiation and propagation.

8. Acknowledgements

The author would like to thank Prof. C Davis for supporting this work, J. E. Garnham for materials and support, R. Ding for FIB support and the EPSRC for funding the work.

9. References

1. ZERBST, U., LUNDÈN, R., EDEL, K. O., SMITH, R. A (2009). *Engineering Fracture Mechanics 76, 2563-2601.*
2. HANS MUSTER, H. S., KLAUS WICK, HENRI PARDIER (1996) Rail rolling contact fatigue. The performance of naturally hard and head-hardened rails in track. *Wear*.
3. F. WETSCHER, R. S., R. PIPPAN (2007) Changes in the mechanical properties of pearlitic steel due to large shear deformation. *Materials science and engineering,* 445-446, 237-243.
4. TELLISKIVI, T., OLOFSSON, U. (2001).Contact mechanics analysis of measured wheel-rail profiles using the finite element method. *Proceedings of the Institution of Mechanical Engineers Part F- Journal of Rail and Rapid Transit, 2, 65-72.*
5. VASIĆ, G., FRANKLIN, F. J., FLETCHER, D. I (2011). Influence of partial slip and direction of traction on wear rate in wheel-rail contact. *Wear 270, 163-171.*
6. IWNICKI, S. (2003) Simulation of wheel-rail contact force. *Fatigue Fracture Engineering Master Structure 26, 887-900. Blackwell Publishing Ltd.*
7. J.E. GARNHAM, C. L. Davis. (2008) The role of deformed rail microstructure on rolling contact fatigue initiation. W*ear*.
8. JIN, N., CLAYTON, P. (1997). Effect of microstructure on rolling/sliding wear of low carbon bainitic steels. *Wear 202, 202-207*.
9. SHARIFF, S. M., PAL, T. K., PADMANABHAM, G. JOSHI, S. V. (2011). Comparative study on Dry Sliding Wear Behaviour of Various Railroad Steels. J*ournal of Tribology, 133*
10. AGLAN, H. A., GAN, Y. X. (2006). Fatigue damage tolerance of bainitic and pearlitic steels. J*ournal of Materials Science, 15, 393-410*
11. CHANG, L. C. (2005) The rolling/sliding wear performance of high silicon carbide-free bainitic steels. *Wear 258, 730-743.*
12. F. J. FRANKLIN, J. E. G., D. J. FLETCHER, C.L. DAVIS, A. KAPOOR (2008) Modelling rail steel microstructure and its effect on crack initiation. W*ear, 265, 1332-1341.*
13. HERNANDEZ, F. C. R., DEMAS, N. G., DAVIS, D. D. (2007). *Mechanical properties and wear of premium rail steels. Wear, 263, 766-772*
14. Image from Computational Thermodynamics Inc.
15. DHUA SK, R. A., SEN SK, PRASAD MS, MISHRA KB, JHA S (2000) Influence of nonmetallic inclusion characteristics on the mechanical properties of rail steel. *Journal of Materials Engineering and Performance,* 9, 700-709.

16. GARNHAM, J. E., DING, R. G., DAVIS, C. L. (2010). Ductile inclusions in rail, subject to compressive rolling-sliding contact. *Wear 296, 733-746*
17. LIU C. D., BASSIM M. N., STLAWRENCE, S. (1993) Evaluation of fatigue crack growth initiation at inclusions in fully pearlitic s teels. *Materials Science and Engineering A Structural Materials Properties Microstructure and Processing, 167, 107-113*
18. ORY, D., DAVIS, C.L (2008). Inclusion density, content and and compostition in a number of rail steels sourced internationally. Summer project – University of Birmingham
19. KIESSLING, R., LANGE, N. (1978) Non-metallic inclusions in steel, *pub. Institute of Materials, UK, (2nd Edition).*
20. J.H. BEYNON, J. E. G., K.J. SAWLEY (1996) Rolling contact fatigue of three pearlitic rail steels. *Wear, 192, 94-111.*
21. GHONEM, H., KALOUSEK, J., STONE, D. H., LAUFER, E. E. (1992) Aspects of plastic deformation and fatigue damage in pearlitic rail steel. *Proceedings of Second International Conference on Heavy Haulage Railway, Colorado Springs. 82-HH-31pp. 339-34*9.